Journal of Hydroinformatics

Journal of Hydroinformatics Vol 26 No 10, 2475 doi: 10.2166/hydro.2024.274

Drone remote sensing to define heat exchange between urban surfaces and stormwater runoff

Greg Dieter and Walter McDonald *

Civil, Construction & Environmental Engineering Department, Marquette University, Milwaukee, WI, USA
*Corresponding author. E-mail: walter.mcdonald@marquette.edu

WM, 0000-0002-9217-7908

ABSTRACT

Urban water bodies are often subject to high runoff temperatures from heat exchange between rainfall and urban surfaces; however, this process can be difficult to define due to the complexity of spatially heterogeneous urban areas. This research seeks to improve our understanding of heat exchange in urban stormwater runoff by integrating *in situ* measurements of runoff temperature with land surface temperature data captured in high spatial resolutions by a drone. To do so, this study monitored four urban catchments in Milwaukee, WI that are dominated by different land surfaces (concrete parking lot, asphalt road, black bitumen roof, and grass). Results indicate that land surface temperature was variable among common land surface types (1.34–2.24 °C), with higher variations in surfaces subject to foot and vehicular traffic. In addition, the temperature of runoff from impervious surfaces responded differently between buildings and those with a ground subsurface, with higher event mean temperatures from concrete (21.4 °C) and asphalt (21.9 °C) ground surfaces as compared with the bitumen roof (19.8 °C), despite similar initial surface temperatures. Ultimately, these outcomes demonstrate how drone remote sensing of land surface temperature and *in situ* monitoring can be integrated to understand heat exchange processes in urban stormwater runoff.

Key words: drone, stormwater runoff, temperature, UAV, urban heat island

HIGHLIGHTS

- Drone (UAS) remote sensing applied to estimate land surface temperatures.
- Remote sensing data assimilated with *in situ* data to evaluate heat exchange in stormwater.
- Land surface temperatures had a higher variation on surfaces subject to traffic.
- Heat exchange in stormwater is distinct between ground and building impervious surfaces.

GRAPHICAL ABSTRACT

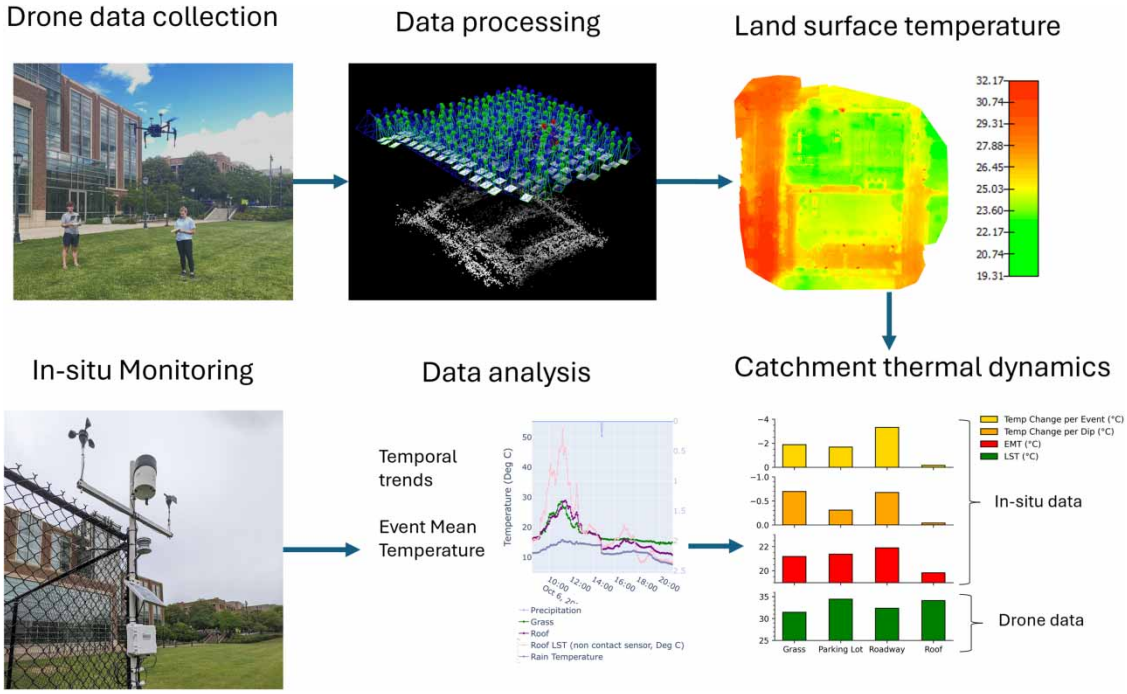

1. INTRODUCTION

The proliferation of impervious surfaces and reduced vegetation within cities has led to urban heat islands, where the temperature of urban areas is higher than surrounding non-developed land. The primary causes of urban heat islands are the prevalence of low albedo surfaces, low evapotranspiration (ET) rates, and anthropogenic heat production (Akbari *et al.* 2001; Stone *et al.* 2010; Jones *et al.* 2012). The resulting higher temperatures can lead to increased energy costs for air conditioning, air pollution, and heat-related illnesses or deaths (Wong *et al.* 2013; Li *et al.* 2019; Piracha & Chaudhary 2022). They also have an environmental impact, such as increased urban water body temperatures from reduced shading, channelization, and increased runoff temperatures (Timm *et al.* 2021). The increased temperatures of urban water bodies are known as the hydrologic urban heat island, where urban streams have comparatively higher baseflow temperatures and are subject to greater temperature surges from stormwater runoff (Zahn *et al.* 2021).

The hydrologic urban heat island can have a profound negative effect on water quality and aquatic health. In urban water bodies, temperature can alter reaction rates, causing an imbalance in important regulating nutrients and compounds. Streams subject to warm urban runoff may contain lower concentrations of dissolved oxygen, impacting respiration and algal production (Butcher 1995; Griffith & Gobler 2020), as well as increased contaminant toxicity (Patra *et al.* 2015). Furthermore, stream temperatures regulate important ecosystem processes, such as fish migration patterns, reproduction, growth, immune responses, and competitive ability (Armour 1991). The importance of stream temperatures to water quality and aquatic health has led to temperature being the top overall impairment in freshwater bodies in several states (Gunawardana & McDonald 2023). Therefore, it is critical to understand the processes that lead to increased stream temperatures from urban stormwater runoff.

It is unclear; however, the degree to which highly heterogenic urban areas contribute to increased stormwater temperatures. Urban areas are spatially complex and contain a variety of land cover types that are subject to different environmental and anthropogenic forces, such as shading from buildings, vehicular traffic, weathering, and pedestrian use. Therefore, estimating the heat exchange in stormwater runoff from urban surfaces is a challenge. Those studies that do exist rely on *in situ* monitoring that capture the heat exchange that occurs within a constrained surface type, location, and conditions (Thompson *et al.* 2008; Herb *et al.* 2009a; Janke *et al.* 2009; Omidvar *et al.* 2018), but may not be representative of land surfaces that are subject to various levels of environmental and anthropogenic effects. It is therefore unclear how

different land cover types contribute to heat exchange in stormwater and what specific urban watershed characteristics control thermal processes in stormwater.

One way to overcome this challenge is through the use of thermal imagery from small unmanned aerial systems (sUAS) or drones that can capture land surface temperature data in high spatial resolutions. Drones are able to supplement *in situ* measurements with data in a high spatial resolution and at on-demand time scales that can provide insights into hydrologic processes within an urban watershed (McDonald 2019). For example, in urban stormwater, drones have been applied to quantify plant stress in urban green stormwater infrastructure (Prettyman *et al.* 2021), measure urban stream velocity (Tauro *et al.* 2016; Shariar *et al.* 2023), determine urban pond geometrics and water ponding (Hassan *et al.* 2023; Zhao *et al.* 2023), and assess stream temperatures (Fitch *et al.* 2018; Kuhn *et al.* 2021). In the context of urban surface temperatures, while *in situ* monitoring limits data collection to discrete points in space, thermal data from drones can provide a spatially distributed estimate of surface temperature (Naughton & McDonald 2019). This data, combined with *in situ* monitoring, can provide additional insights into the influence of surface temperatures on stormwater runoff.

The objective of this study is to understand the impact that the composition of catchment surfaces has on heat transfer in urban stormwater runoff. To meet this objective, this study monitors four urban catchments that are dominated by different land surfaces (concrete parking lot, asphalt road, black bitumen roof, and grass). Monitoring includes both *in situ* monitoring of stormwater runoff at the catchment outlet using water level, acoustic Doppler velocimeter, and temperature sensors, as well as thermal imagery from a sUAS before and after storm events. Integrating this data together, this study presents a novel approach to evaluate the effect that land surface temperatures of specific land cover types have on heat exchange in stormwater runoff. Doing so provides a greater understanding of heat exchange in urban stormwater systems that can be used to target mitigation measures to protect downstream water quality and human health.

2. METHODS

2.1. Site description

This study monitored four small urban catchments located in Milwaukee, WI (Figure 1), including a parking lot (concrete, 2,500 m^2), roadway (hot mix asphalt pavement, 1,100 m^2), roof (rubber membrane, 175 m^2), and small urban greenspace (grass, 2,200 m^2). Additional catchment characteristics are listed in Supplementary Table SI-1. Monitoring occurred over July through October 2022 during which 14 storms were observed.

2.2. *In situ* monitoring

In situ equipment included spatially discrete, temporally continuous data loggers that monitored temperature, runoff, and atmospheric conditions (Supplementary Figures SI-1–SI-4). Devices to measure temperature and runoff were placed at the outlet of each catch basin. Temperature loggers were created using EnviroDIY Mayfly Data Logger boards, 64 gigabyte microSD cards, uxcell 6 V 60 mA Mini Solar Cells, 3.7v lithium polymer batteries, and temperature sensors. Runoff flow rates were captured with two types of sensors: Global Water Instruments flow loggers and ISCO 2150 loggers. Global Water WL 400 water level sensors that measure both temperature and flow depth were placed at the catch basin outlet (i.e., curb inlet or grate inlet) and were programmed to collect at 5-min intervals. Two ISCO 2150s that capture water level and velocity were placed within the sewer network below selected catch basins to validate the water balance. The ISCO 2150s use acoustic Doppler velocimetry and were programmed to log data at 5-min intervals. Finally, an Onset HOBO temperature/relative humidity sensor, wind speed and direction sensor, and precipitation bucket were installed within the greenspace catchment.

2.3. sUAS monitoring

Land surface temperature was captured using a DJI M100 drone with a Zenmuse XTR thermal camera and flights were performed using Pix4Dcapture software. Flights took approximately 15 min at 300 ft with an overlap of 90%, depending on weather conditions. The Pix4D desktop application was then used to stitch the individual land surface temperature images into a single mosaic and the data were spatially processed and analyzed using ArcGIS Pro and Python. In addition, land surface temperature was validated using spot measurements from a FLIR TG54 Spot infrared sensor. The sUAS captured land surface temperature at a high resolution both before and after storm events and throughout the day to capture diurnal trends in land surface temperature. To capture land surface temperature before storm events, the sUAS was deployed prior to when rainfall would begin based on a variety of weather forecasts. To capture the diurnal trends in land surface temperature, sUAS

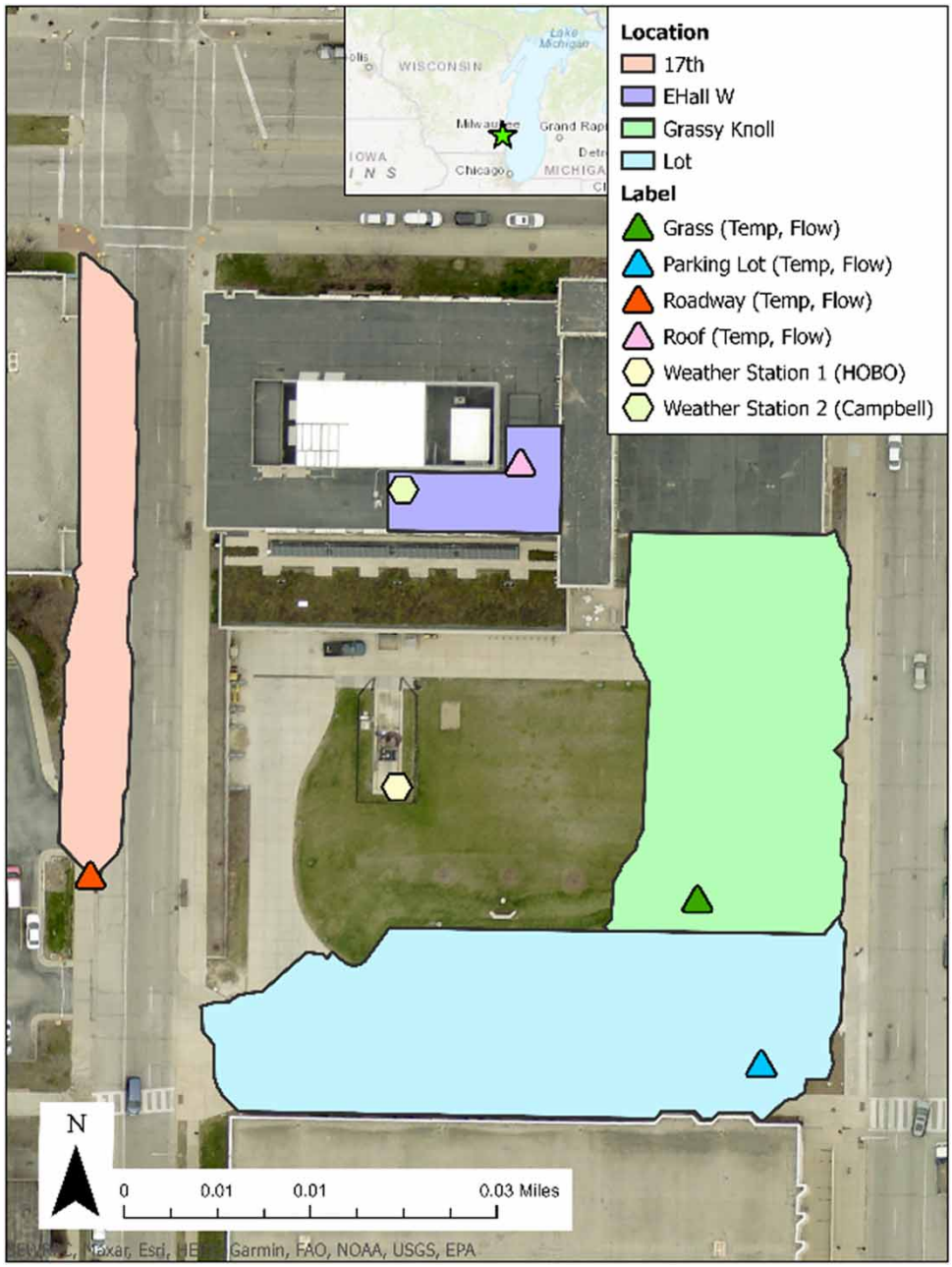

Figure 1 | Catchments in Milwaukee, WI including the location of *in situ* sensors.

flights were performed at 09:00, 12:00, 15:00, and 17:00 across three representative summer days: (1) a hot summer day, (2) a cool summer day, and (3) an overcast summer day (Supplementary Figure SI-8).

2.4. Data processing and analysis

2.4.1. *In situ* data

From the *in situ* data, three analyses were performed to analyze the characteristics of each runoff event including analysis of (1) the temporal relationship between wet bulb (rain), surface, and runoff temperature, (2) the change in runoff temperature during discrete runoff events, and (3) the event mean temperature (EMT) of each storm.

First, the runoff temperature was plotted with computed rainfall temperature and land surface temperature to analyze how runoff temperature compares to rain and surface temperature as storms proceed. The rain temperature was estimated by using

wet bulb temperature (van Buren *et al.* 2000; Herb *et al.* 2009a; Omidvar *et al.* 2019), which represents the minimum temperature reached when an unsaturated parcel of air is cooled via evaporation at a constant pressure and is dependent on air temperature and relative humidity conditions (Monteith & Unsworth 2013):

$$T_{\text{wb}} = T * \arctan\left(0.15 * (\text{RH} + 8.31)^{\frac{1}{2}}\right) + \arctan(T + \text{RH}) - \arctan(\text{RH} - 1.68) + 3.9E - 3(\text{RH})^{\frac{3}{2}} * \arctan(2.3E - 2{*}\text{RH}) - 4.69 \quad (1)$$

where T_{wb} represents the wet bulb temperature, T represents the air temperature in degrees Celsius, and RH represents the relative humidity percent (Vecellio *et al.* 2022). The wet bulb temperature was assumed to be representative of the temperature of rainfall; therefore, the difference between the observed runoff temperature and the rain (wet bulb) temperature was then plotted to observe whether heat export was present.

Next, the behavior of runoff temperature during an event was computed by calculating the number of fluctuations, or dips, in temperature during precipitation events and the overall magnitude of temperature change. This was done because in the beginning of an event, the runoff temperature is usually highest due to the initial small depth of runoff and high rate of heat exchange between the land surface and runoff. Over the course of an event, runoff temperature typically decreases due to an increase in the flow rate or volume of stormwater runoff, and then subsequently increases as flow rates decrease (Herb *et al.* 2009a). These fluctuations, or dips, can inform both the hydrologic timing of heat exchange, as well as the magnitude of heat exchange that occurs between the surface and runoff. To define these dips in the temperature time series, precipitation events were first segmented and defined using a 1-h antecedent dry period and an initial rainfall volume of 0.01 inches. Overall differences in runoff temperature were calculated by subtracting the initial temperature from the final temperature. Finally, within these events, the number and magnitude of temperature dips in were counted, defined as the presence of a local decrease in runoff temperature concurrent with a local precipitation peak.

Lastly, EMT was computed for each storm to estimate the average runoff temperature of each event. EMT is a flow-weighted average runoff temperature defined as follows:

$$\text{EMT} = \frac{\sum Q * T}{\sum Q} \quad (2)$$

where Q represents the flow rate and T represents the runoff temperature. EMT was used as a metric to compare the thermal impact across catchments of different land cover compositions and sizes. Other approaches include estimating overall thermal load (Herb *et al.* 2009b; Jones *et al.* 2009); however, thermal loads are difficult to compare between catchments due to the varying size of catchments and subsequent volumes of runoff, and therefore, EMT provides a volume-weighted approach to compare runoff temperatures across catchments.

Two methods were used for calculating Q, depending on the monitoring data available at the selected site. The first method calculated Q directly using depth and velocity data from the ISCO sensors placed at the outlet of the parking lot site. Where direct flow rate data was not available, Q was calculated using the rational method:

$$Q = C * i * A \quad (3)$$

where C is the runoff coefficient, i is the rainfall intensity, and A is the runoff area. A composite runoff coefficient was computed for each catchment according to the following:

$$C_{\text{composite}} = \frac{\sum C * A}{\sum A} \quad (4)$$

based on the area of each land cover type within the catchment (Supplementary Table SI-2).

2.4.2. sUAS data

Land surface temperature images were processed using Pix4D to stitch the thermal images into a single orthomosaic. This orthomosaic was then emissivity corrected based upon the Stefan–Boltzmann law to ensure an accurate temperature for each land surface type:

$$T_{ec} = \sqrt[4]{\frac{T_{ls}^4 - (1-\varepsilon)T_a^4}{\varepsilon}} - 273.15 \quad (5)$$

where T_{ec} is emissivity corrected temperature (degrees Celsius), T_{ls} is the land surface temperature (degrees Kelvin), ε is emissivity, and T_a is air temperature (degrees Kelvin) (Blonquist *et al.* 2009). Next, the orthomosaic was georeferenced in ArcGIS Pro using nine control points, and a polygon feature layer containing land use types was created to match the corresponding mosaic boundaries that may change between data collection periods. For example, parked cars in roadways and parking lots were always in different locations between flights. The final product is a land surface temperature raster in degrees Celsius that is emissivity corrected on a land cover basis within the four catchments of interest: parking lot, roadway, grass, and rooftop. Finally, zonal statistics were performed on this data to determine the mean and variance of land surface temperature of land covers within each catchment.

3. RESULTS AND DISCUSSION

3.1. *In situ* data

Data were collected between July and October 2022, during which 14 storms were captured. During some of the storm events, there was incomplete data due to several factors including power failure, sensor errors, or theft. In particular, the roadway sensors were stolen at the end of August; therefore, the *in situ* data presented is segmented based on data availability. A complete list of available *in situ* data for each storm event is provided in Supplementary Table SI-7. This data was used to evaluate the temporal characteristics of runoff temperatures, their inter-event dynamics, and the EMT in the following sections.

3.1.1. Temporal analysis

The temporal behavior of temperatures was first analyzed by plotting the *in situ* runoff and rainfall temperatures and quantifying the degree to which runoff temperatures changed throughout a rain event. First, the temperatures of the Arduino sensor were plotted over time to observe their responses to runoff events. These sensors were installed at the interface of the land surface and the air above the surface; therefore, prior to runoff these sensors represent a composite temperature of the surface and air temperatures, while during runoff they are assumed representative of the runoff for which they are submerged. This is highlighted in Figure 2, which provides an example of runoff temperatures for two of the catchments: roof and grass. This figure shows that before the storm event, the roof temperature is consistently 2 °C above the rainfall temperature (Figure 2(a)); however, as the runoff event begins, there is a sharp decrease in roof runoff temperature as it captures initial rainfall, and then fluctuates before converging to a similar temperature. Similarly, the grass catchment (Figure 2(b)) exhibits sharp decreases corresponding to high intensity precipitation rates, but the runoff temperature decreases much slower from a difference of about 3–2 °C above the rainfall temperature (Figure 2(b)).

After observing these initial behaviors, we sought to quantify the change in runoff temperature over the course of a storm event. To do so, the difference in runoff temperature between the beginning and end of all observed storm events was computed (Figure 3 and Supplementary Table SI-4). Figure 3 represents the distribution of changes in runoff temperature from the beginning to end of each storm event. Figure 3(a) illustrates temperature changes in runoff over the entire study period of July–October ($n = 14$) for every catchment but the roadway, as this sensor was stolen midway through sampling. However, to assess all land uses, data from July to August ($n = 6$) are shown in Figure 3(b) during which all sensors were deployed. As illustrated in Figure 3(a), all three catchments – parking lot, roof, and grass – had negative median runoff temperature differences, suggesting that the runoff has cooled from a warmer temperature. Interestingly, for the data constrained to July–August, the median change in roof temperature during this time was close to zero. This could be due to the unique thermal characteristics of the roof and impact that diurnal trends in temperature have on observed temperature changes (Supplementary Figure SI-8), where precipitation events that start in the early evening or morning, and end at mid-day, demonstrate an overall increase in temperature due to the impact of rising air temperatures and solar radiation.

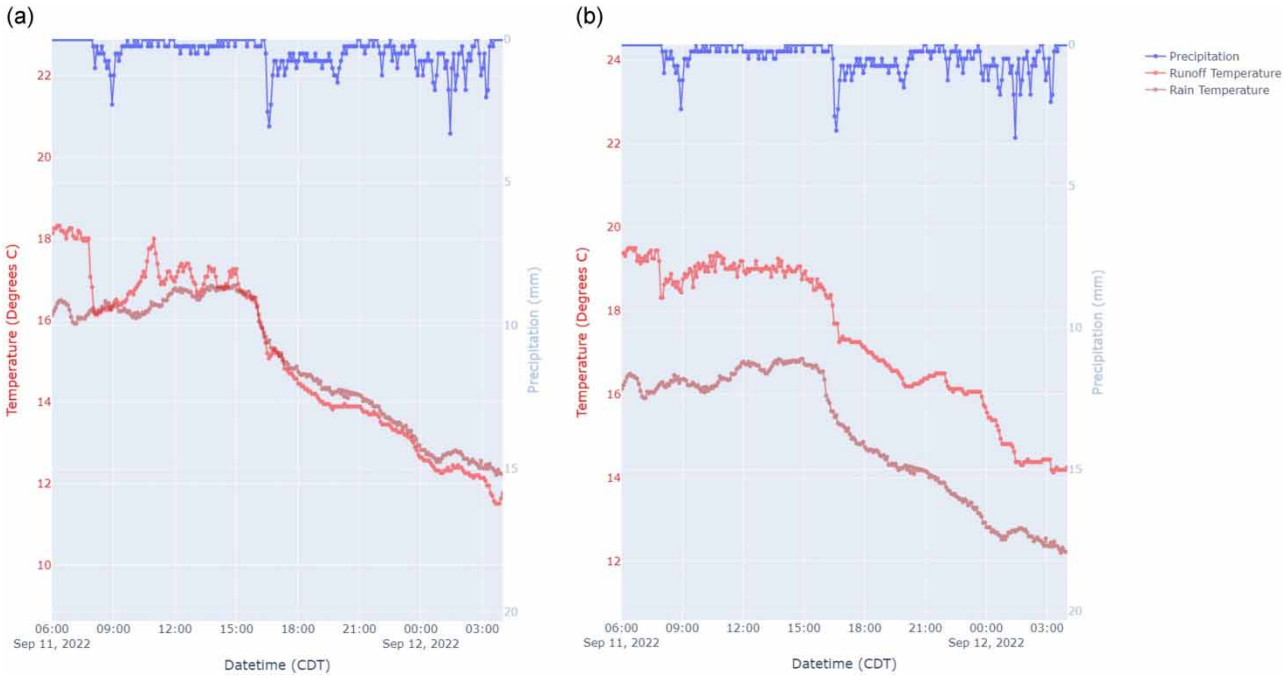

Figure 2 | Representative rainfall and runoff temperature figure for the 9 November 2022 storm event for the (a) roof and (b) grass catchments.

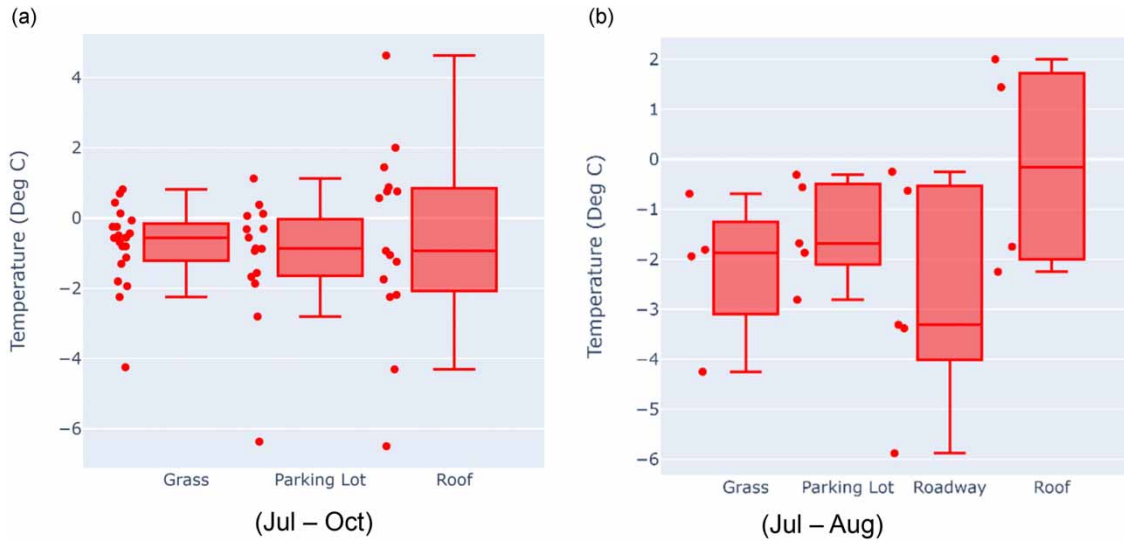

Figure 3 | Boxplot of runoff temperature differences computed for (a) all monitored storm events and (b) only storm events in July and August.

3.1.2. Intra-event temperature dynamics

Based upon the time series plots, it was apparent that rainfall did not happen in a uniform distributed manner, but that storms produced multiple pulses of rainfall that resulted in distinct runoff and temperature responses (e.g., Figure 4). Therefore, to further analyze the extent of heat exchange during precipitation events, these unique intra-event temperature fluctuations, or 'dips' in temperature were characterized. To do so, the intra-event temperature fluctuations were analyzed by (1) counting the number of dips within each storm event and (2) estimating average magnitude of these dips.

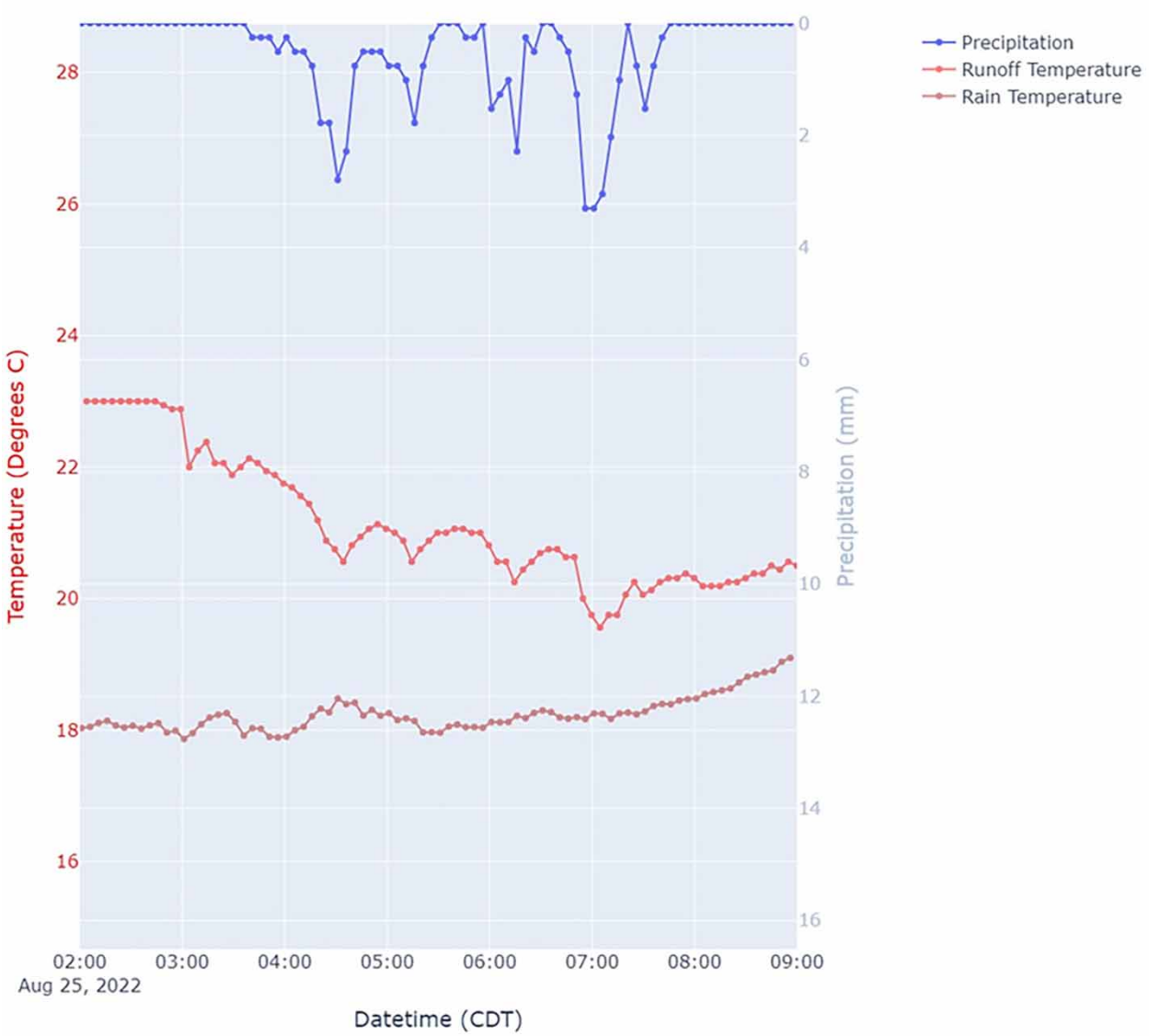

Figure 4 | Example of temperature fluctuations throughout a storm event due to interspersed pulses of rainfall.

The number of energy export dips within each storm event, and the average magnitude of each dip are illustrated in Figure 5. While the roadway and parking lot had similar dip counts, the parking lot had several storms for which the number of dips was low. This difference could be due to catchment characteristics; the parking lot (1,800 m^2) is over twice as large as the roadway (600 m^2) and a smaller catchment could therefore exhibit more runoff temperature fluctuations due to increased hydrologic responsiveness and smaller time of concentration. To define the magnitude of the intra-event fluctuations in temperature, the median degree change per export event (dip) was calculated. For the data constrained between July and August (Figure 5(b)), the roadway and grass catchments had the highest median average degree change per event (−0.68 and −0.69 °C), followed by the parking lot (−0.31 °C) and the roof catchments (−0.04 °C). Meanwhile, the grass had the highest standard deviation degree change per dip (1.88 °C), followed by the roof (1.22 °C), roadway (0.56 °C), and parking lot (0.33 °C) (Supplementary Table SI-5).

Overall, these results indicate that catchments are distinct in their intra-event energy exchange response to rainfall. The roadway catchment typically experiences the greatest energy export dip counts and magnitudes. While the grass has a high change in temperature per dip, it also has the lowest number of dips per storm, possibly due to the high time of concentration (Supplementary Table SI-1); therefore, even though the grass has a similar temperature change per dip as the roadway,

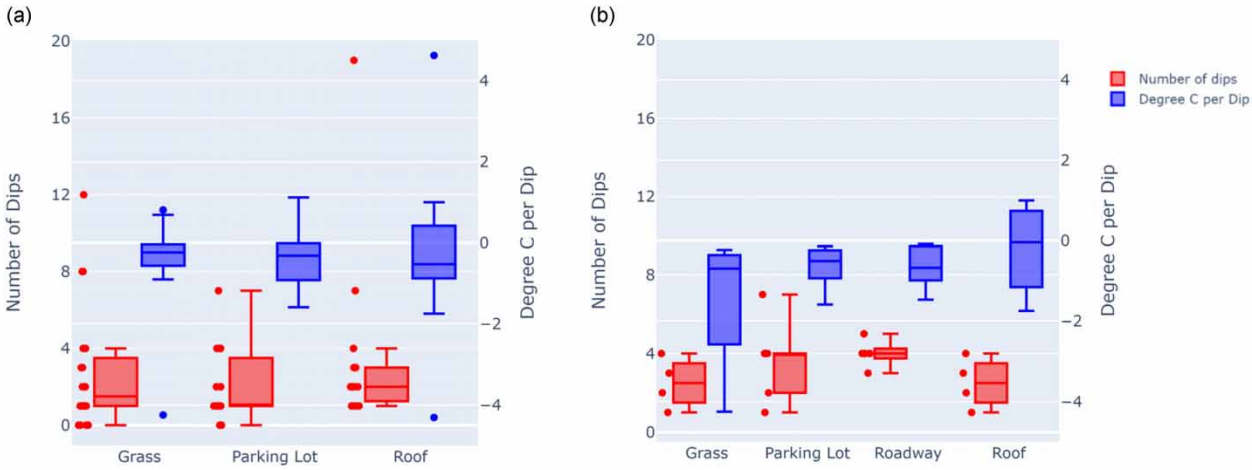

Figure 5 | Boxplots of the number of dip events (left axis) and the degrees Celsius change per dip (right axis) for (a) all monitored storm events and (b) only storm events in July and August.

it has less frequent fluctuations in temperature. Finally, the roof catchment had the lowest temperature change per dip and a high standard deviation, possibly due to the air-conditioned subsurface, leading to more rapid thermal equilibrium between the roof surface and the runoff temperatures.

3.1.3. Event mean temperature

EMT was computed to compare the overall thermal impact between catchments and across seasons. The EMT analysis found (1) distinct responses between catchments and (2) that the rooftop exhibited low EMTs despite the high magnitude temporal metrics from previous analyses. The road site exhibited the highest EMT (median 21.9 °C), followed by the parking lot (median 21.4 °C), grass (median 21.2 °C), and roof (19.8 °C) (Figure 6(b)). These results align with the temperature change and dip analysis: the highest EMT is being produced by the roadway, which was identified as having the greatest temperature change across and within an event.

The parking lot exhibited higher EMT than the roof catchment during summer months (Figure 6(b)) despite having comparable overall temperature changes (e.g., Figures 3 and 4). This indicates that the parking lot is prone to high land surface

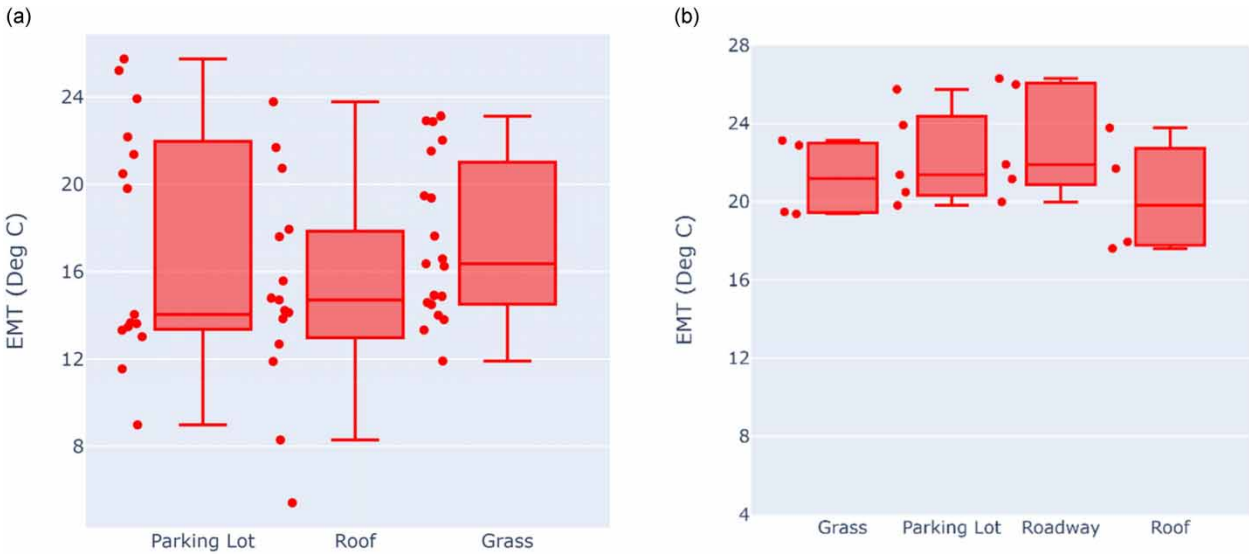

Figure 6 | Event mean temperature (EMT) for all storms captured at the parking lot, roof, and grass catchment (a) and for those storms captured in July to August (b).

temperatures similar to the roadway catchment, but intra-event dynamics that govern thermal equilibrium and thermal load operate differently, perhaps due to catchment characteristics. On the other hand, the roof catchment produced low EMT and low intra-event dynamics. This could be due to the roof subsurface being cooler than a terrestrial subsurface, leading to a quicker thermal equilibrium and therefore lower land surface temperature as rain events proceed.

3.2. sUAS data

Thermal imagery from a sUAS was collected periodically before and after storm events (flight details are in Supplementary Table SI-9). An example of the thermal data is illustrated in Figure 7. As illustrated, there is a wide degree of variation in the land surface temperature across land cover types. This temperature data from each flight was then used to develop summary statistics of temperature for each distinct land cover type and within each catchment.

A high-level summary of the distribution of the standard deviation and median land surface temperatures observed for all flights within each catchment is illustrated in Figure 8(a) and 8(b). From Figure 8(b), the roadway produced the highest median land surface temperature, followed by the parking lot and roof, and lastly the grass catchment. These results follow the *in situ* results, which found the roadway to have the highest energy export and EMT, the parking lot to have higher EMTs than the roof, and the highest variability of temperature in the roof catchment.

To further define land surface temperature variability, the standard deviations of both the complete catchments and individual surface types were quantified using the sUAS land surface temperature data (Figure 8(a)). The parking lot exhibited the widest interquartile range of 1.22 °C and highest median of standard deviations at 2.24 °C. The roadway catchment has the lowest interquartile range, but second highest median. The *in situ* analysis found that the roadway has the highest energy export and EMT values, and these results indicate the standard deviation of the roadway catchment land surface temperature is also the most consistent. Overall, the roof and grass catchments exhibited the lowest standard deviations, which may be because these catchments are more homogeneous than the other catchments; the roadway and parking lot are made up of fragmented medians, concrete, asphalt, canopy cover, etc., compared with the roof and grass catchments which are continuously a roof or grass cover, respectively. Their surface homogeneity leads to more consistent land surface temperatures throughout the catchments. In addition, categorized by specific land cover type (Supplementary Figure SI-6), natural land cover types (e.g., grass and shrub/mulch) catchments had lower variations in temperature than impervious surface types (e.g., asphalt and pavement).

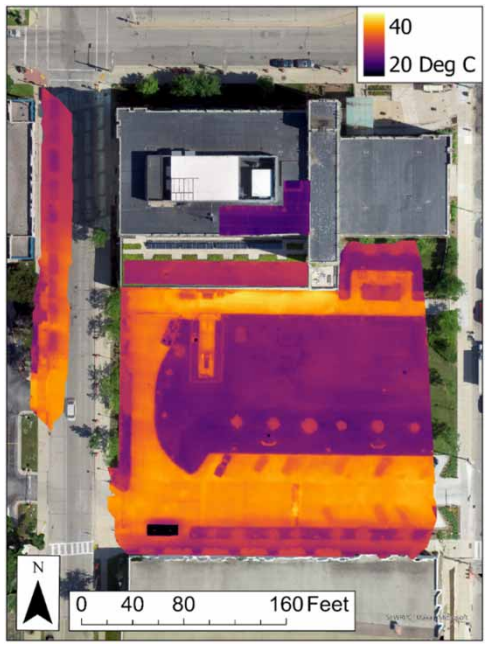

Figure 7 | Example of temperature data from sUAS flight on 24 August 2022 at 19:45.

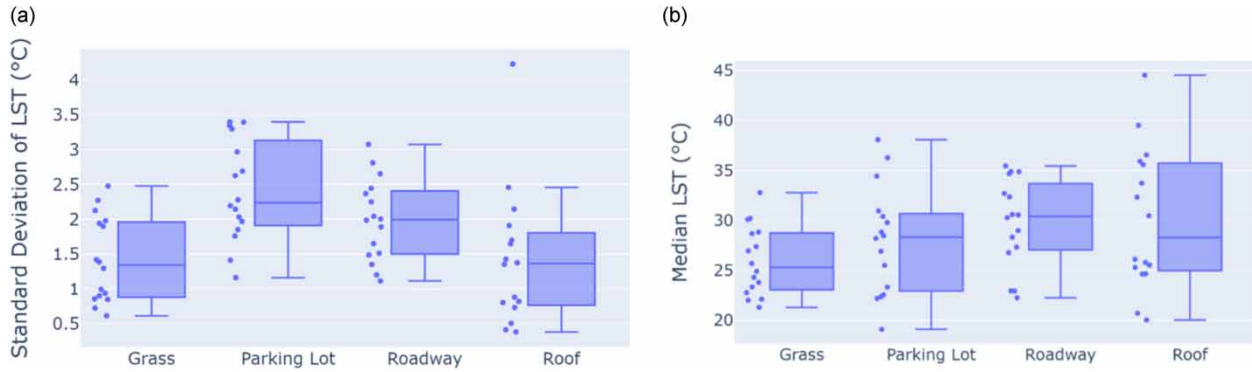

Figure 8 | Distribution of (a) land surface temperature (LST) standard deviations (°C) and (b) median land surface temperature (°C).

3.3. Key metrics

To compare key metrics from *in situ* and sUAS data, median temperature change per event, temperature change per dip, EMT, and land surface temperature from July to August are presented in Figure 9. The data presented is restricted to dates in July and August for which both *in situ* data and land surface temperature data prior to a storm event are available. Comparing the median land surface temperature to *in situ* temperatures provides unique observations on the behavior of the individual catchments. The roadway produced the highest *in situ* metrics (e.g., overall temperature change and EMT), yet its median land surface temperature prior to the storms was less than both the parking lot and the roof. In addition, while the roof had the highest median land surface temperature, it produced the lowest temperature changes and EMT. Finally, while the grass had the lowest median land surface temperature, its median *in situ* metrics appear to be similar or higher than the parking lot catchment. Therefore, there is not a clear trend between runoff temperature metrics and land surface temperatures; a high land surface temperature does not guarantee high runoff temperature trends.

3.4. Discussion and implications of results

This research presents a novel sUAS and *in situ* remote monitoring approach that demonstrates distinct thermal variability of urban surfaces during stormwater runoff. The monitoring campaign captured rainfall, runoff, and temperature data of four

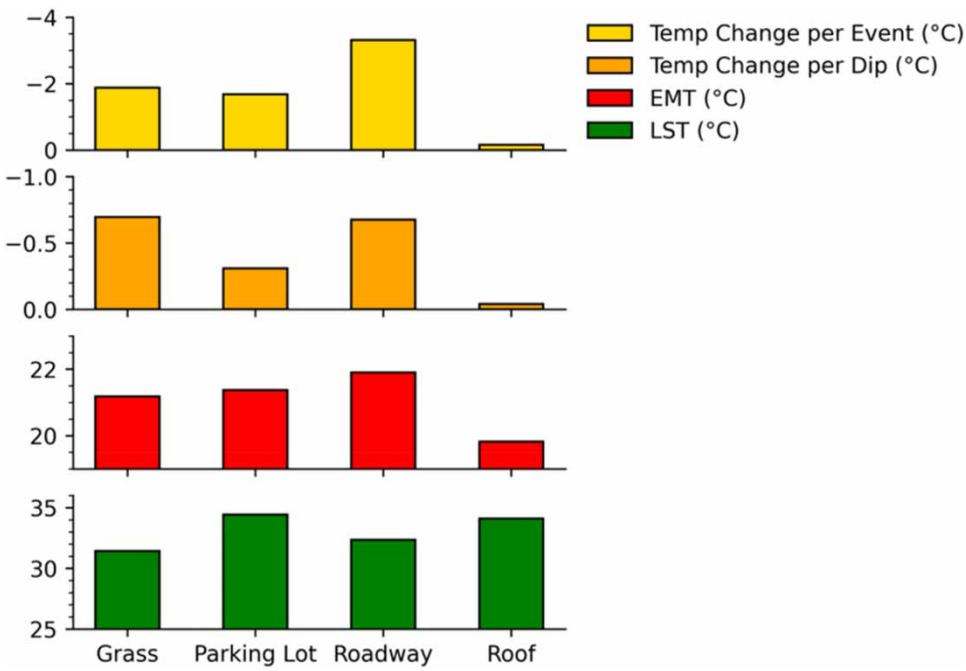

Figure 9 | Comparison of key *in situ* and sUAS medians from July to August.

urban catchments using *in situ* and sUAS methods to compare trends in temporal thermal response, intra-event energy exchange dynamics, EMT, and spatial variability due to differences in catchment composition. The results show urban catchments have a high degree of spatial variability in land surface temperatures due to their unique catchment compositions, leading to distinct temporal responses.

Over the course of storm events, runoff temperatures decreased but remained higher than rainfall temperature, indicating that runoff was exporting stored energy from the surface of the catchments. These temperature changes happened at different rates throughout each catchment and are likely dependent on catchment characteristics such as time of concentration and catchment size; thermal characteristics such as albedo and subsurface energy fluxes; and storm characteristics such as magnitude and duration. The roadway catchment experienced the most energy loss across storm events, the most frequent energy export events within storm events, and the highest EMT. This is likely due to the catchment characteristics, such as the second smallest drainage area, high imperviousness (95%), and low albedo.

In this study, the temperature of runoff from impervious surfaces responded differently between buildings and those with a ground subsurface. While the roof exhibited one of the highest initial land surface temperatures, it consistently produced the lowest EMTs. These trends are due to the rapid thermal responsiveness exhibited by the surface, which produces steep energy exchanges at the beginning of storm events that plateau at a low thermal equilibrium. These responses are likely due to the presence of a weaker and cooler subsurface energy flux, unlike the other three terrestrial catchments. Therefore, the overall thermal impact of impervious surfaces is not equivalent across impervious surfaces due to the quicker cooling of roof surfaces as compared with ground-based impervious surfaces (e.g., roads, sidewalks, and parking lots).

Catchments and land surfaces exhibited different ranges of land surface temperatures and land surface temperature variability from the sUAS data, even for those land surfaces of similar types. For example, concrete surfaces responded with different land surface temperatures and standard deviations across the roadway, grass, and parking lot catchments. Additionally, similar surfaces exchanged energy at different rates between catchments demonstrated by the distinct standard deviations of temperature differences due to storm events. These results indicate a land surface temperature as an effective parameter (i.e., assuming that it is the same across an entire land cover type) could misrepresent the energy exchange dynamics due to unique surface characteristics such as local shading, age of surface, and traffic loading, among others.

From this study, there were advantages and limitations to using thermal imagery from a sUAS to evaluate heat transfer in the catchments. An advantage was the collection of surface temperature data in high spatial resolutions that can overcome overly generalized assumptions of surface temperatures and properly capture variability of land surface temperatures within a catchment. However, this data was limited by the temporal resolution of the data, which required the ability to fly the sUAS in adequate weather conditions. Temporal analyses of land surface temperature change and diurnal periodicity highlighted how imprecise flight times leave land surface temperatures vulnerable to diurnal periods. However, this vulnerability is not ubiquitous across catchments; the rapid thermal responsiveness of the roof catchment led to faster land surface temperature changes in the absence of rainfall and presence of clear skies. Precise flight times corresponding to storm events would minimize the potential skew introduced by a diurnal period, although the diurnal period of storm days is subdued and less extreme as compared with a hot and clear day.

The results from this study can be used to inform effective implementation of best management practices (BMPs) to mitigate high runoff temperatures. BMPs such as green stormwater infrastructure have been shown to reduce runoff temperatures (Timm *et al.* 2020; Gunawardana *et al.* 2023; Bodus *et al.* 2024), but it may not be clear where the best locations for implementation would be for reducing downstream temperatures. From these results, it is clear that impervious surfaces on the ground (i.e., roadway and parking lot catchments) produce higher thermal impacts than those that represent the roof of buildings (i.e., roof catchment). Therefore, if reducing thermal impacts of stormwater runoff is a primary goal, BMPs might be more effective in treating stormwater runoff from impervious surfaces at the ground level, rather than those that collect runoff from buildings.

4. CONCLUSION

This paper presents a unique monitoring study that integrates *in situ* and remote sensing of temperature to evaluate the heat exchange in stormwater runoff from urban surfaces. Results indicate that runoff temperatures decreased but remained higher than rainfall temperature, indicating runoff was exporting stored energy from the surface of the catchments. Land surface temperature data from drones indicated a wide variability in temperature among common land surfaces (1.34–2.24 °C),

with a higher variation in surfaces subject to foot and vehicular traffic. In addition, the temperature of runoff from impervious surfaces responded differently between buildings and those with a ground subsurface, with higher event mean temperatures from concrete (21.4 °C) and asphalt (21.9 °C) ground surfaces as compared with the bitumen roof (19.8 °C), despite higher initial surface temperatures of the roof. Future work could apply the proposed approach to further define the factors that contribute to differences in runoff temperature between impervious surfaces of buildings and those with a ground subsurface. Ultimately, these outcomes help to improve our understanding of heat transfer in stormwater runoff within complex urban systems and can help to guide the implementation of BMPs to protect downstream water bodies.

DATA AVAILABILITY STATEMENT

Data cannot be made publicly available; readers should contact the corresponding author for details.

CONFLICT OF INTEREST

The authors declare there is no conflict.

REFERENCES

Akbari, H., Akbari, H., Pomerantz, M. & Taha, H. (2001) Cool surfaces and shade trees to reduce energy use and improve air quality in urban areas. **70** (3), 295–310.

Armour, C. L. (1991) *Guidance for Evaluating and Recommending Temperature Regimes to Protect Fish*, Vol. 90. US Department of the Interior, Fish and Wildlife Service. Fort Collins, Colorado, USA.

Blonquist, J. M., Norman, J. M. & Bugbee, B. (2009) Automated measurement of canopy stomatal conductance based on infrared temperature, *Agricultural and Forest Meteorology*, **149** (11), 1931–1945. https://doi.org/10.1016/j.agrformet.2009.06.021.

Bodus, B., Malley, K. O., Dieter, G., Gunawardana, C. & Mcdonald, W. (2024) Review of emerging contaminants in green stormwater infrastructure : Antibiotic resistance genes, microplastics, tire wear particles, PFAS, and temperature, *Science of the Total Environment*, **906** (June 2023). https://doi.org/10.1016/j.scitotenv.2023.167195.

Butcher, J. B. (1995) Dissolved-oxygen analysis with temperature dependence, *Journal of Environmental Engineering*, **121** (10), 756–759.

Fitch, K., Kelleher, C., Caldwell, S. & Joyce, I. (2018) Airborne thermal infrared videography of stream temperature anomalies from a small unoccupied aerial system, *Hydrological Processes*, **32** (16), 2616–2619. https://doi.org/10.1002/hyp.13218.

Griffith, A. W. & Gobler, C. J. (2020) Harmful algal blooms: A climate change co-stressor in marine and freshwater ecosystems, *Harmful Algae*, **91**, 101590.

Gunawardana, C. & McDonald, W. (2023) The influence of socioeconomic and spatial variables on total maximum daily load progress in the United States, *Water Policy*, **25**(11), 1062–1078. https://doi.org/10.2166/wp.2023.112.

Gunawardana, C., Dupasquier, M. & McDonald, W. (2023) Green infrastructure in series reduces thermal impacts of stormwater runoff, *Journal of Sustainable Water in the Built Environment*, **9** (2), 5023001.

Hassan, S. Z., Sun, P., Gokgoz, M., Chen, J., Reinhart, D. R. & Gustitus-Graham, S. (2023) UAV-based approach for municipal solid waste landfill monitoring and water ponding issue detection using sensor fusion, *Journal of Hydroinformatics*, **25**(6), 2107–2127

Herb, W. R., Janke, B., Mohseni, O. & Stefan, H. G. (2009a) Runoff temperature model for paved surfaces, *Journal of Hydrologic Engineering*, **14** (10), 1146–1155. https://doi.org/10.1061/(asce)he.1943-5584.0000108.

Herb, W. R., Mohseni, O. & Stefan, H. G. (2009b) Simulation of temperature mitigation by a stormwater detention pond, *Journal of the American Water Resources Association (JAWRA)*, **45** (5), 1164–1178. https://doi.org/10.1111.

Janke, B. D., Herb, W. R., Mohseni, O. & Stefan, H. G. (2009) Simulation of heat export by rainfall-runoff from a paved surface, *Journal of Hydrology*, **365** (3–4), 195–212. https://doi.org/10.1016/j.jhydrol.2008.11.019.

Jones, M. P., Asce, M. & Hunt, W. F. (2009) Bioretention impact on runoff temperature in trout sensitive waters, *Journal of Environmental Engineering*, **135** (8), 577–585. https://doi.org/10.1061/ASCEEE.1943-7870.0000022.

Jones, M. P., Hunt, W. F. & Winston, R. J. (2012) Effect of urban catchment composition on runoff temperature, *Journal of Environmental Engineering*, **138** (12), 1231–1236. https://doi.org/10.1061/(asce)ee.1943-7870.0000577.

Kuhn, J., Casas-Mulet, R., Pander, J. & Geist, J. (2021) Assessing stream thermal heterogeneity and cold-water patches from UAV-based imagery: A matter of classification methods and metrics, *Remote Sensing*, **13** (7), 1379.

Li, X., Zhou, Y., Yu, S., Jia, G., Li, H. & Li, W. (2019) Urban heat island impacts on building energy consumption: A review of approaches and findings, *Energy*, **174**, 407–419.

McDonald, W. (2019) Drones in urban stormwater management: A review and future perspectives, *Urban Water Journal*, **16** (7), 505–518. https://doi.org/10.1080/1573062X.2019.1687745.

Monteith, J. L. & Unsworth, M. H. (2013) *Principles of Environmental Physics: Plants, Animals, and the Atmosphere*, 4th edn. Academic Press; Oxford, UK. Available at: http://elsevier.com/locate/permissions.

Naughton, J. B. & McDonald, W. M. (2019) Evaluating the variability of urban land surface temperatures using drone observations, *Remote Sensing*, **11**(14), 1722.

Omidvar, H., Song, J., Yang, J., Arwatz, G., Wang, Z. H., Hultmark, M., Kaloush, K. & Bou-Zeid, E. (2018) Rapid modification of urban land surface temperature during rainfall, *Water Resources Research*, **54** (7), 4245–4264. https://doi.org/10.1029/2017WR022241.

Omidvar, H., Bou-Zeid, E. & Chiaramonte, M. (2019) Physical determinants and reduced models of the rapid cooling of urban surfaces during rainfall, *Journal of Advances in Modeling Earth Systems*, **11** (5), 1364–1380. https://doi.org/10.1029/2018MS001528.

Patra, R. W., Chapman, J. C., Lim, R. P., Gehrke, P. C. & Sunderam, R. M. (2015) Interactions between water temperature and contaminant toxicity to freshwater fish, *Environmental Toxicology and Chemistry*, **34** (8), 1809–1817.

Piracha, A. & Chaudhary, M. T. (2022) Urban air pollution, urban heat island and human health: A review of the literature, *Sustainability*, **14** (15), 9234.

Prettyman, K., Babbar-sebens, M., Parrish, C. E. & Babbar-sebens, J. M. (2021) A feasibility study of uninhabited aircraft systems for rapid and cost-effective plant stress monitoring at green stormwater infrastructure facilities, *Journal of Hydroinformatics*, **23** (3), 417–437. https://doi.org/10.2166/hydro.2020.195.

Shariar, J., Medeiros, H., Sebo, S. & Mcdonald, W. (2023) River velocity measurements using optical flow algorithm and unoccupied aerial vehicles : A case study, *Flow Measurement and Instrumentation*, **91** (February), 102341. https://doi.org/10.1016/j.flowmeasinst.2023.102341.

Stone, B., Hess, J. J. & Frumkin, H. (2010) Urban form and extreme heat events: Are sprawling cities more vulnerable to climate change than compact cities? *Environmental Health Perspectives*, **118** (10), 1425–1428. https://doi.org/10.1289/ehp.0901879.

Tauro, F., Porfiri, M. & Grimaldi, S. (2016) Surface flow measurements from drones, *Journal of Hydrology*, **540**, 240–245.

Thompson, A. M., Wilson, T., Norman, J. M., Gemechu, A. L. & Roa-Espinosa, A. (2008) Modeling the effect of summertime heating on urban runoff temperature, *Journal of the American Water Resources Association*, **44** (6), 1548–1563. https://doi.org/10.1111/j.1752-1688.2008.00259.x.

Timm, A., Ouellet, V. & Daniels, M. (2020) Swimming through the urban heat island: Can thermal mitigation practices reduce the stress? *River Research and Applications*, **36** (10), 1973–1984. https://doi.org/10.1002/rra.3732.

Timm, A., Ouellet, V. & Daniels, M. (2021) Riparian land cover, water temperature variability, and thermal stress for aquatic species in urban streams, *Water*, **13** (19), 2732.

van Buren, M. A., Watt, W. E., Marsalek, J. & Anderson, B. C. (2000) Thermal enhancement of stormwater runoff by paved surfaces, *Water Resources*, **34** (4), 1359–1371.

Vecellio, D. J., Wolf, S. T., Cottle, R. M. & Kenney, W. L. (2022) Evaluating the 35°C wet-bulb temperature adaptability threshold for young, healthy subjects (PSU HEAT Project), *Journal of Applied Physiology*, **132** (2), 340–345.

Wong, K. V., Paddon, A. & Jimenez, A. (2013) Review of world urban heat islands: Many linked to increased mortality, *Journal of Energy Resources Technology*, **135** (2), 22101.

Zahn, E., Welty, C., Smith, J. A., Kemp, S. J., Baeck, M. & Bou-Zeid, E. (2021) The hydrological urban heat island: Determinants of acute and chronic heat stress in urban streams. *JAWRA Journal of the American Water Resources Association*, **57**(6), 941–955.

Zhao, G., Rasmussen, M. R., Larsen, K. G., Srba, J., Nielsen, T. D., Goorden, M. A. & Nielsen, J. E. (2023). Determine stormwater pond geometrics and hydraulics using remote sensing technologies: A comparison between airborne-LiDAR and UAV-photogrammetry field validation against RTK-GNSS. *Journal of Hydroinformatics*, **25**(4), 1256–1275.

First received 21 November 2023; accepted in revised form 2 September 2024. Available online 1 October 2024